

Enhanced wavelength-dependent surface tension of liquid–vapour interfaces

F. Höfling and S. Dietrich

Max-Planck-Institut für Intelligente Systeme, Heisenbergstraße 3, 70569 Stuttgart, Germany, and
IV. Institut für Theoretische Physik, Universität Stuttgart, Pfaffenwaldring 57, 70569 Stuttgart, Germany

Due to the simultaneous presence of bulk-like and interfacial fluctuations the understanding of the structure of liquid–vapour interfaces poses a long-lasting and ongoing challenge for experiments, theory, and simulations. We provide a new analysis of this topic by combining high-quality simulation data for Lennard-Jones fluids with an unambiguous definition of the wavenumber-dependent surface tension $\gamma(q)$ based on the two-point correlation function of the fluid. Upon raising the temperature, $\gamma(q)$ develops a maximum at short wavelengths. We compare these results with predictions from density functional theory. Our analysis has repercussions for the interpretation of grazing-incidence small-angle X-ray scattering (GISAXS) at liquid interfaces.

PACS numbers: 68.03.Hj, 61.20.Ja, 05.10.-a

Introduction.— In a simple fluid, liquid (ℓ) and vapour (v) phases can coexist at temperatures between those of the triple point and the ℓ - v critical point, $T_t \leq T \leq T_c$. A planar ℓ - v interface gives rise to a free energy $\gamma_0 A$ in excess of the bulk free energy; A is the interface area and γ_0 the macroscopic surface tension between the two coexisting bulk phases. The interface is spatially broadened by the simultaneous occurrence of bulk-like fluctuations of the local number density and of thermally excited capillary wave (CW)-like fluctuations [1–3] (fig. 1a). The free energy cost of the latter has been predicted to depend on their wavenumber q and has been expressed in terms of a q -dependent surface tension $\gamma(q)$ entering into an effective interface Hamiltonian \mathcal{H}_{int} [4–6], which allows one to calculate the spatial structure of the interface. Within density functional theory (DFT), a pronounced minimum of $\gamma(q)$ was found as a consequence of the omnipresent van der Waals forces between the molecules of the fluid [6]: $\gamma(q \rightarrow 0) = \gamma_0 + aq^2 \ln(qb) + O(q^4)$ with $a > 0$ [4] and a length b . The initial non-analytic decrease reflects the asymptotic decay $\sim r^{-6}$ of the pair potential. The length b is determined by compressibility effects in the interfacial region and thus it is sensitive to microscopic details of the interaction; it controls both the position $q_{\text{min}} = (b\sqrt{e})^{-1}$ of the minimum and its depth. Evidence for such a minimum has been obtained experimentally from GISAXS on the ℓ - v interface of water [7], other molecular fluids [8], and liquid gallium [9]. The variation of $\gamma(q)$ signals that, depending on their wavelength, interfacial fluctuations are either *favoured* or *suppressed* with potentially far-reaching implications for nanoparticle probes [10, 11], wetting films [12], and droplet nucleation [13]. Although liquid droplets are *a priori* distinct from flat interfaces, their surface tension varies with the radius [3, 14, 15] and one may expect a related non-analyticity therein for long-ranged interactions [16, 17].

In simulations, a *decrease* of $\gamma(q)$ for decreasing wavelength $2\pi/q$ has been observed for polymeric liquids [18, 19] and for colloidal suspensions [20–22]; an *increase* has been found for water [23] and simple fluids [24]. These studies are based on short-ranged interactions and yield monotonic functions $\gamma(q)$ so that the aforementioned min-

imum could not be corroborated by simulations so far. New evidence for untruncated Lennard-Jones (LJ) fluids near T_t suggests that there is indeed a shallow minimum [25]. These simulation data have almost always been analysed in terms of the height fluctuations of the local position $\hat{z}(\mathbf{R})$ of an intrinsic interface as considered also within DFT studies. It requires interpreting a given configuration of particle positions $\{\mathbf{r}_j = (\mathbf{R}_j, z_j)\}_{j=1, \dots, N}$ in terms of a fluctuating interface $\hat{z}(\mathbf{R})$ with an associated intrinsic density profile, i.e., the microscopic number density at point $\mathbf{r} = (\mathbf{R} = (x, y), z)$ is assumed to take the form $\hat{\rho}(\mathbf{R}, z) = \hat{\rho}_{\text{int}}(z - \hat{z}(\mathbf{R}))$. The definition of $\hat{z}(\mathbf{R})$ is not unique, leading to an ambiguity in $\gamma(q)$ [5, 26]. Even the qualitative shape of $\gamma(q)$ depends on the choice of $z(\mathbf{R})$ [27, 28]: for a LJ fluid, the local version of Gibbs’ dividing surface (GDS) criterion yields a *decreasing* $\gamma(q)$, while $\gamma(q)$ *increases* monotonically if a many-particle definition is employed [24]. Such kind of ambiguities have to drop out from expressions for interface-related physical observables. In particular, scattering data do not depend on various notions of an intrinsic interface.

Here, we discuss $\gamma(q)$ in terms of the interface structure factor $H(q)$. It allows one to extract $\gamma(q)$ from GISAXS data without additional assumptions concerning the sample or choosing specific models for it. Our simulation results enrich the physical picture of ℓ - v interfaces considerably: Near the triple point, $\gamma(q; T \approx T_t)$ is almost flat over a wide q -range. Sweeping T from T_t to the critical point T_c , $\gamma(q; T)$ shows a significant enhancement and develops a maximum at short wavelengths. This behaviour can be rationalised in terms of a length scale which grows upon approaching T_c .

Definition of $\gamma(q)$.— The structure of the ℓ - v interface separating the coexisting bulk phases is characterised by the two-point density correlation function [1] $G(|\mathbf{q}|, z, z') = \int d^2R e^{-i\mathbf{q}\cdot\mathbf{R}} [\langle \hat{\rho}(\mathbf{0}, z) \hat{\rho}(\mathbf{R}, z') \rangle - \rho(z)\rho(z')]$ in planar geometry; $\mathbf{q} = (q_x, q_y)$ is the lateral wavevector, and the mean density profile $\rho(z) = \langle \hat{\rho}(\mathbf{R}, z) \rangle$ interpolates between the number densities ρ_ℓ and ρ_v of the coexisting phases (fig. 1b). Although $G(q, z, z')$ is not directly accessible to experiments, information on it can be obtained from GISAXS: the scattered intensity for a lateral

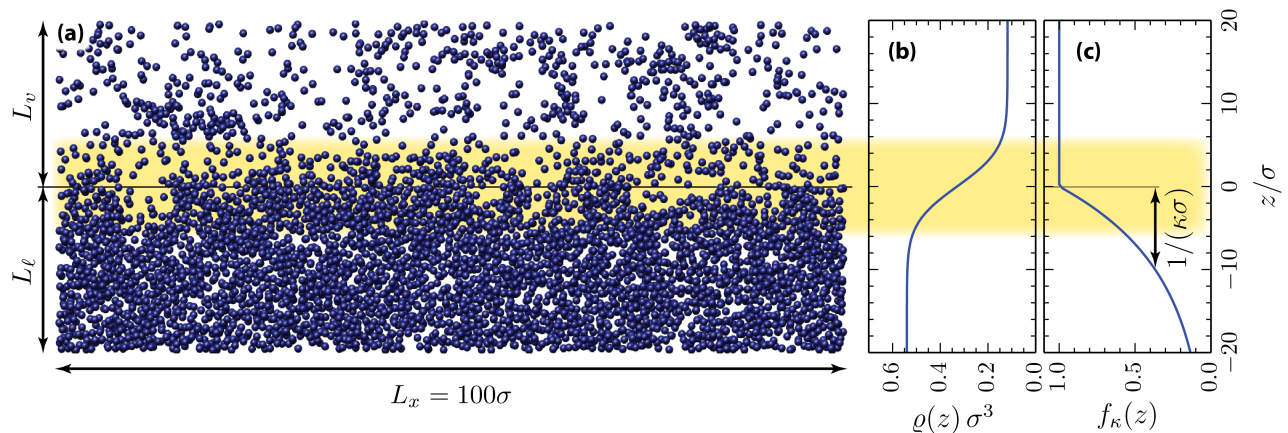


Figure 1. Simulation snapshot of the ℓ - v interface for a LJ fluid at $T^* = 1.15$. A vertical slice of width 3.5σ and height 40σ is shown with the interfacial region highlighted (panel a); σ is the particle diameter. Panel (b) displays the corresponding mean density profile $\rho(z)$ and panel (c) the weight function $f_\kappa(z)$ used to compute the GISAXS intensity from eq. (1) for $\kappa\sigma = 0.1$.

scattering vector \mathbf{q} is proportional to [eq. (2.68) in ref. 29]

$$I_{\text{tot}}(\mathbf{q}; \kappa) = \iint dz dz' f_\kappa(z)^* f_\kappa(z') G(\mathbf{q}, z, z'), \quad (1)$$

omitting reflection and transmission coefficients. The function $f_\kappa(z)$ depends on the scattering geometry, i.e., the angles α_i and α_f of incidence and detection, respectively. For X-rays entering from the vapour side, $f_\kappa(z)$ describes the decay of the associated evanescent wave on the liquid side, $f_\kappa(z < 0) = \exp(-\kappa|z|)$ with the penetration depth $1/\kappa(\alpha_i, \alpha_f)$ [29, 30] (fig. 1c). Here, $z = 0$ indicates the position of the GDS for $\rho(z)$. Due to the low number density of the vapour, we take $f_\kappa(z > 0) = 1$; for improvements see ref. [29]. For α_i and α_f close to the critical angle of total reflection, the X-rays penetrate the sample deeply ($\kappa \rightarrow 0$) and the total scattered intensity $I_{\text{tot}}(q; \kappa) = I_b(q; \kappa) + I_{\text{int}}(q; \kappa)$ contains a sizeable contribution $I_b(q; \kappa)$ from bulk fluctuations on top of the interfacial one, $I_{\text{int}}(q; \kappa)$. A sufficiently large penetration depth $1/\kappa \gg \zeta$ is required in order to obtain complete information on the interface of width ζ ; if the interfacial region probed is too shallow, (rare) CWs with a large amplitude are not captured by the X-rays. The bulk scattering intensity $I_b(q; \kappa) = I_b^{(\ell)}(q; \kappa) + I_b^{(v)}(q)$ is determined by $G(q, z, z')$ for $|z|, |z'| \rightarrow \infty$, i.e., by the familiar structure factors $S_\alpha(k)$ (see below) of both phases $\alpha = \ell, v$ [c.f., eq. (5)]; in particular, one finds that the liquid side yields $I_b^{(\ell)}(q; \kappa) = \rho_\ell S_\ell(q)/(2\kappa) + O(\kappa^0)$ as $\kappa \rightarrow 0$. On the other hand, the interface part $I_{\text{int}}(q; \kappa)$ has to become independent of the penetration depth as $\kappa \rightarrow 0$, which motivates and facilitates the definition of an interface structure factor $H(q)$ as $I_{\text{int}}(q; \kappa) = H(q) + O(\kappa)$, which is equivalent to

$$H(q) := \lim_{\kappa \rightarrow 0} [I_{\text{tot}}(q; \kappa) - I_b(q; \kappa)]. \quad (2)$$

Upon construction, $H(q)$ is specified by $G(q, z, z')$ alone. It summarises the modifications of the local density dis-

tribution caused by the presence of the interface.

Next, we consider $H(q \rightarrow 0)$ within classical CW theory, which—in the absence of an external potential—predicts a divergence of $G(q \rightarrow 0, z, z') \simeq k_B T \rho'(z) \rho'(z') / (\gamma_0 q^2)$ [1, 31–33]. We insert this into eqs. (1) and (2) and use that $I_{\text{tot}}(q; \kappa) = I_b(q; \kappa) + O(\kappa^0)$ as $\kappa \rightarrow 0$ for q fixed and that $I_b(q; \kappa)$ is bounded in q for κ fixed. Since $q^2 I_{\text{int}}(q; \kappa)$ is regular for $\kappa, q \rightarrow 0$ one finds asymptotically [34]

$$H(q \rightarrow 0) \simeq k_B T (\Delta\rho)^2 [\gamma_0 q^2]^{-1}, \quad (3)$$

where $\Delta\rho := \rho_\ell - \rho_v$. For $\kappa\zeta \ll 1$ but fixed, $H(q)$ dominates the scattering intensity as $q \rightarrow 0$: $I_{\text{tot}}(q; \kappa) = H(q) + O(q^0)$. Thus in principle, γ_0 can be inferred from $I_{\text{tot}}(q \rightarrow 0; \kappa)$ directly. We generalise eq. (3) to arbitrary q , such that $\gamma(q \rightarrow 0) = \gamma_0$, by *defining* a q -dependent surface tension

$$\gamma(q) := k_B T (\Delta\rho)^2 [q^2 H(q)]^{-1}. \quad (4)$$

Therefore, $H(q)$ and $\gamma(q)$ are equivalent descriptions of the interface structure, both determined by $G(q, z, z')$.

Bulk contribution.— The bulk contribution $I_b(q; \kappa)$ follows from the corresponding expression for $G_b(q, z, z')$ entering eq. (1). The bulk reference system is formed by two independent, macroscopically large half-spaces $z < 0$ and $z > 0$ filled with the coexisting liquid and vapour phase, respectively; the bulk structures are taken to be unperturbed by the sharp boundary at $z = 0$. Thus $G_b(q, z, z')$ equals the bulk functions $G_\alpha(q, |z - z'|)$ if z and z' are on the same side of the interface ($zz' > 0$) and $G_b(q, z, z') = 0$ otherwise; $G_\alpha(q, |z - z'|)$ is related uniquely to $S_\alpha(|\mathbf{k}|) = \rho_\alpha^{-1} \int_{-\infty}^{\infty} e^{-ik_z u} G_\alpha(|\mathbf{q}|, u) du + \rho_\alpha (2\pi)^3 \delta(\mathbf{k})$ for $\mathbf{k} = (\mathbf{q}, k_z)$. All correlations between particles located on opposite sides of the interface are contained exclusively in $H(q)$, and $I_b(q; \kappa)$ is the sum of the scattered intensities from the two half-spaces. For simulations, the finiteness of the scattering volume of

height L_α for either phase (fig. 1b) must also be taken into account, leading to [34]

$$I_b^{(\alpha)}(q; \kappa) = \varrho_\alpha \int_{-\infty}^{\infty} \frac{dk_z}{2\pi} \frac{S_\alpha(\sqrt{q^2 + k_z^2})}{\kappa^2 + k_z^2} \times [1 + e^{-2\kappa L_\alpha} - 2e^{-\kappa L_\alpha} \cos(k_z L_\alpha)] \quad (5)$$

up to a term $\propto \delta(\mathbf{q})$; for $\alpha = v$, $\kappa = 0$. Concerning the interpretation of future GISAXS data, the second line is replaced by unity ($L_\alpha \rightarrow \infty$).

It is instructive to inspect the asymptotics of $I_b^{(\alpha)}$ with respect to the non-commuting limits $\kappa \rightarrow 0, L_\alpha \rightarrow \infty$ [34]:

$$I_b^{(\alpha)}(q; \kappa) \simeq \frac{1 - e^{-2\kappa L_\alpha}}{2\kappa} \varrho_\alpha S_\alpha(q) + (1 + e^{-2\kappa L_\alpha}) \varrho_\alpha \mathcal{I}_0^{(\alpha)}(q)$$

up to terms $O(\kappa)$, $e^{-\kappa L_\alpha} O(L_\alpha^{-1})$. Taking $L_\ell \rightarrow \infty$ first, the first term on the l.h.s. describes the singularity of the bulk scattering from the liquid side: $I_b^{(\ell)}(q; \kappa) \simeq \varrho_\ell S_\ell(q)/(2\kappa)$ as $\kappa \rightarrow 0$. If $\kappa \rightarrow 0$ first (as for $\alpha = v$), $I_b^{(\alpha)}(q; \kappa) \simeq \varrho_\alpha L_\alpha S_\alpha(q)$ as $L_\alpha \rightarrow \infty$. The next order $\sim (\kappa L)^0$ contains $\mathcal{I}_0^{(\alpha)}(q) := \int dk_z [S_\alpha(\sqrt{q^2 + k_z^2}) - S_\alpha(q)]/(2\pi k_z^{-2})$, which are bounded functions of q . According to eq. (2), these terms contribute to $H(q)$, and it is crucial that the full expression for $I_b(q; \kappa)$ is used therein. In particular, adopting a definition for $G_b(q, z, z')$ and thus $I_b(q; \kappa)$ different from eq. (5) affects $\gamma(q)$. Whereas the leading terms of $I_b(q; \kappa)$ and $I_{\text{tot}}(q; \kappa)$ must coincide, there is no such constraint for the next order. For example, including bulk-like correlations due to the presence of the interface, $G_b(q, z, z') \neq 0$ for $zz' < 0$, modifies $\gamma(q)$ by a term $O(q^2)$ [26]. Previous interpretations of GISAXS experiments [7, 8] approximated $I_b^{(\ell)}(q; \kappa) \approx \varrho_\ell S_\ell(0)/(2\kappa)$, which for $\gamma(q)$ implies an extra factor of $1 + q^2(\gamma_0/k_B T)(\Delta\varrho)^{-2} \varrho_\ell \mathcal{I}_0^{(\ell)}(0) + O(q^4)$; it reduces $\gamma(q)$ if $\mathcal{I}_0^{(\ell)}(0) < 0$.

Simulation method. — For LJ fluids we have performed molecular dynamics (MD) simulations of a flat liquid slab coexisting with its vapour phase. The LJ pair potential $V(r) = 4\epsilon [(r/\sigma)^{-12} - (r/\sigma)^{-6}]$ is truncated and shifted to zero at $r_c = 3.5\sigma$ (not 2.5σ as usual). The investigated dimensionless temperatures range from $T^* := k_B T/\epsilon = 0.70$ slightly above $T_t^* \approx 0.68$ [35] up to $T^* = 1.15 \approx 0.94 T_c^*$. We have estimated $T_c^* \approx 1.22$ from the linear extrapolation to 0 of $(\Delta\varrho)^{1/\beta}$ as function of T , using $\beta = 0.327$ [36, 37]. Since we are interested, *inter alia*, in small q , large simulation boxes containing several 10^5 particles are needed. Powerful means for such demanding simulations are provided by the highly parallel architecture of modern graphics processors (GPUs). We have used the software *HAL's MD package* (version 0.3) [38], which delivers accurate and efficient, GPU-accelerated MD simulations.[39] The geometry of the simulation box is given by the total height $L_z = L_\ell + L_v$ and the cross-sectional area $\mathcal{A} = L_x L_y$; the total number of particles N fixes the ratio L_ℓ/L_v via

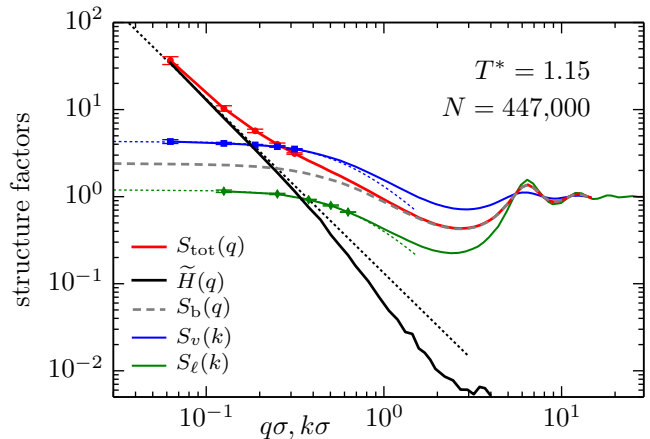


Figure 2. Decomposition of $S_{\text{tot}}(q) = (\mathcal{A}/N)I_{\text{tot}}(q; \kappa \rightarrow 0)$ for the inhomogeneous system ($L_\ell = 50\sigma, L_v = 3L_\ell$) into the interface structure factor $\tilde{H}(q) = (2\mathcal{A}/N)H(q)$ and the bulk contribution $S_b(q)$. The latter follows from the structure factors $S_\ell(k)$ and $S_v(k)$ of the coexisting bulk phases [eq. (5)]; the bulk data are extrapolated to $k = 0$ by an Ornstein–Zernike fit (green and blue dotted lines). Solid lines connect actual data points. The black dotted line, which is approached by $\tilde{H}(q \rightarrow 0)$, indicates the prediction of classical CW theory [eq. (3)].

the GDS criterion $N/\mathcal{A} = \varrho_\ell L_\ell + \varrho_v L_v$. Two parallel, on average flat ℓ - v interfaces of total area $A = 2\mathcal{A}$ have been prepared by bringing separately equilibrated, coexisting bulk phases into spatial contact (with periodic boundary conditions in all directions). We have used liquid slabs of width $L_\ell = 25\sigma$ ($T^* \leq 1.0$) or 50σ ($T^* \geq 1.1$), $L_x = L_y = 100\sigma$, and $L_z = 125\sigma$ or 200σ . In the next step, the thermally excited CWs have been equilibrated by MD runs lasting $3\text{--}10 \times 10^3 \tau$ with $\tau = (m\sigma^2/\epsilon)^{1/2}$ and particle mass m . The production runs have covered at least $15 \times 10^3 \tau$, and averages over $10\text{--}30$ independent runs have been taken. In order to minimise disk access we have used the H5MD file format [40] and have evaluated all relevant observables *in situ*, e.g., $I_{\text{tot}}(|\mathbf{q}|; \kappa) = \langle |\hat{\varrho}_\kappa(\mathbf{q})|^2 \rangle / \mathcal{A}$ where $\hat{\varrho}_\kappa(\mathbf{q}) = \sum_{j=1}^N f_\kappa(z_j) e^{i\mathbf{q}\cdot\mathbf{R}_j}$ is computed after each interval τ . Further, we introduce the dimensionless quantities[41] $S_{\text{tot}}(q) := (\mathcal{A}/N)I_{\text{tot}}(q; \kappa \rightarrow 0)$, $S_b(q) := (\mathcal{A}/N)I_b(q; \kappa \rightarrow 0)$, and $\tilde{H}(q) := S_{\text{tot}}(q) - S_b(q) = (2\mathcal{A}/N)H(q)$.

Figure 2 illustrates the determination of $\tilde{H}(q)$ for $T^* = 1.15$. The total structure factor $S_{\text{tot}}(q)$ displays a steep increase for $2 \gtrsim q\sigma \rightarrow 0$, and at $q = 2\pi/L_x$ it exceeds the height of the first peak of the liquid structure by a factor of ca. 27. Nevertheless, it barely displays the CW asymptote $\sim q^{-2}$ [eq. (3)]. The bulk contribution $S_b(q)$ is computed via eq. (5) with $S_\ell(k)$ and $S_v(k)$ obtained from separate simulations of homogeneous systems at $\varrho_\ell \sigma^3 = 0.540$ and $\varrho_v \sigma^3 = 0.118$. The functions $S_\alpha(k)$ are extrapolated to $k = 0$ using the Ornstein–Zernike form $S_\alpha(k) \simeq \varrho_\alpha k_B T \chi_\alpha / [1 + (k\xi_\alpha)^2]$ by fitting the bulk

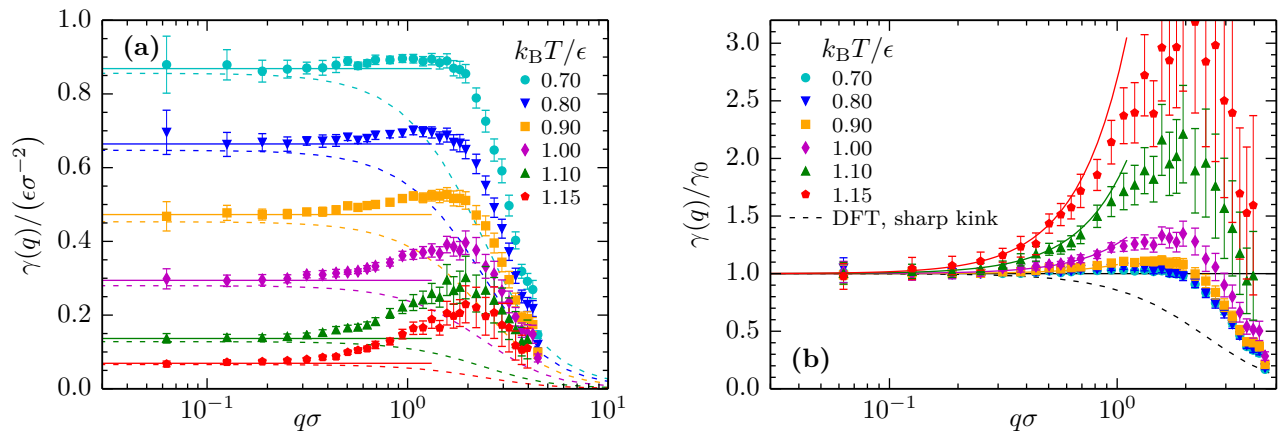


Figure 3. Wavenumber-dependent surface tension $\gamma(q)$ of LJ fluids with truncated interaction range ($r_c = 3.5\sigma$) as extracted from $\tilde{H}(q)$ according to eq. (4). (a) Solid horizontal lines indicate the macroscopic surface tensions $\gamma_0(T)$ determined via the mechanical route. Dashed lines represent the simulation-enhanced DFT prediction [see the main text and eq. (7)]; $\gamma_0(T)$ from MD simulations and from theory differ slightly at low T . (b) The same data for $\gamma(q)$ normalised by $\gamma_0(T)$; full lines are fits of a quadratic increase [eq. (6)]. The black dashed line shows the DFT prediction within the sharp-kink approximation [4].

compressibilities χ_α and the correlation lengths ξ_α . The highly compressible vapour phase contributes about 70% to $S_b(q \rightarrow 0)$ and must not be ignored; it still adds 22% at $T^* = 0.70$. [42] For $q\sigma \gtrsim 3$, the bulk part $S_b(q)$ resembles $S_{\text{tot}}(q)$ with a deviation of less than 1%. The signal of $\tilde{H}(q)$ is visible over more than 3 decades and clearly approaches and follows the CW divergence as $q \rightarrow 0$ [eq. (3), fig. 2]. The only parameter left unspecified is γ_0 , which we have determined independently via the mechanical route [1]. With this, the whole procedure does not involve any adjustable parameter.

Results for $\gamma(q)$.— The q -dependent surface tension follows from eq. (4). We have generated high-quality data for $\gamma(q; T)$ for temperatures T covering almost the whole two-phase coexistence region and for wavenumbers q spanning 2 decades (fig. 3a). Upon raising T^* from 0.70 to 1.15, the macroscopic surface tension $\gamma_0(T)$ decreases by a factor of 12. The concomitant reduction of $\gamma(q)$ is, however, not uniform for all q : it is only about a factor of 4 for $q\sigma \approx 2$, leading to an *enhancement* of $\gamma(q)$ relative to γ_0 . The strong T -dependence can be accounted for by studying $\gamma(q)/\gamma_0$ (fig. 3b). At $T^* = 0.70$, i.e., close to the triple point, $\gamma(q)/\gamma_0 \approx 1$ for $q\sigma \lesssim 2$ and $\gamma(q)$ is nearly independent of q . As T is raised, our data for $\gamma(q)$ change from an almost flat to an initially increasing function. For $q\sigma \gtrsim 2$, the surface tension is found to again decrease as a function of q . Thus on route towards T_c , $\gamma(q)$ develops a *maximum* at $q_{\text{max}}(T)$, which shifts from $q_{\text{max}}\sigma \approx 1.0$ to 2.1 as T^* increases from 0.8 to 1.15. The maximum value is enhanced over γ_0 by a factor of ca. 3 for $T^* = 1.15$. The function $\gamma(q)$ is analytic in q^2 due to $r_c < \infty$ and its initial increase can be described by an emerging length $\ell(T)$:

$$\gamma(q; T)/\gamma_0(T) = 1 + [q\ell(T)]^2 + O(q^4), \quad q \rightarrow 0. \quad (6)$$

The coefficient $\mathcal{K} = \gamma_0\ell^2$ has often been interpreted as a bending rigidity of the interface; it has been shown within DFT for \mathcal{H}_{int} that \mathcal{K} summarises compressibility effects of the coexisting phases [6]. Along these lines, the length ℓ may be viewed as an effective cutoff $q < 2\pi/\ell$ of the CW spectrum, which reduces the interface roughness. [28]. For $T^* \geq 0.8$, we find $\ell(T)$ to be comparable to the bulk correlation lengths ξ_ℓ and ξ_v . The latter diverge as $\xi_\alpha \sim |t|^{-\nu}$ with $\xi_\ell/\xi_v \rightarrow 1$, $\nu \approx 0.630$, $t := (T - T_c)/T_c \rightarrow 0$ [36, 37], and $\gamma_0 \sim |t|^{2\nu}$ [37, 43]. For $T^* \leq 1.15$, we find $\xi_\alpha \lesssim 1.5\sigma$ so that one cannot assign a power law to these data. If nonetheless one anticipates the same scaling for $\ell(T)$ and $\ell/\xi_\alpha \rightarrow 1$, this implies $\mathcal{K}(T \rightarrow T_c) = (4\pi\omega)^{-1}k_B T_c$, where $\omega \approx 0.87$ is a universal number [15, 44]. Our data corroborate this scaling of \mathcal{K} ; however, it is at variance with earlier predictions [21, 22].

A pressing issue is the absence (in simulations) of the local minimum in $\gamma(q)$ observed experimentally [7–9] and predicted theoretically [6] for fluids governed by *bona fide* dispersion forces decaying $\sim r^{-6}$. Any interaction cutoff r_c converts the corresponding non-analytic contribution $q^2 \ln(qb)$ in $\gamma(q)$ into a term $-q^2 \ln(r_c/b)$, which competes with the aforementioned term $(q\ell)^2$. However, $\gamma(q)$ is expected to not change qualitatively once r_c is sufficiently large ($q \gtrsim 2\pi/r_c$). From recent simulations of LJ fluids, a shallow minimum near $q_{\text{min}} \approx 0.24\sigma$ ($b \approx 2.5\sigma$) has indeed been identified within a suitable extrapolation scheme for $r_c \rightarrow \infty$ [25]. This is not accessible from our data.

Simulations of GISAXS.— Within the MD simulations, we have also determined $I_{\text{tot}}(q; \kappa)$ for a range of penetration depths $1/\kappa$ as it would be observed in GISAXS experiments. To this end, we define $\gamma_{\text{eff}}(q; \kappa)$ analogously to eq. (4), therein replacing $H(q)$ by $I_{\text{int}}(q; \kappa)$. It is crucial that both the finite-size effects and $\kappa > 0$ are properly included in $I_b(q; \kappa)$ [eq. (5)]. The data in fig. 4 support

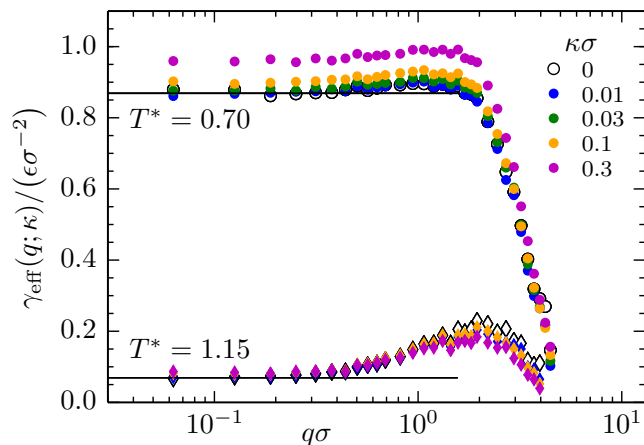


Figure 4. Dependence of $\gamma_{\text{eff}}(q; \kappa)$ on the penetration depth $1/\kappa$ at two temperatures. These results are based on the GISAXS intensity $I_{\text{tot}}(q; \kappa)$ obtained on the fly from the MD simulations. The data for $\kappa = 0$ (open symbols) are reproduced from fig. 3.

our mathematical finding that $\gamma_{\text{eff}}(q; \kappa \rightarrow 0) = \gamma(q)$. The increase of $\gamma_{\text{eff}}(q \rightarrow 0; \kappa)$ upon increasing κ agrees quantitatively with the difference $I_{\text{int}}(q; \kappa) - H(q) = O(\kappa\zeta)$. The data for the present LJ fluids indicate that $\kappa\sigma \lesssim 0.03$ is small enough to yield a reliable approximation of $\gamma(q)$.

Simulation-enhanced DFT.— For comparison with DFT predictions based on an effective interface Hamiltonian \mathcal{H}_{int} [6], we start from the systematic expansion of $\gamma(q)$ in terms of q but neglect the Gaussian curvature contribution to the intrinsic density profile (i.e., $C_H = 0$ in the notation of ref. [6]) because the corresponding terms in $\gamma(q)$ are not amenable to a quantitative evaluation within our simulations. The DFT expression left involves only $\varrho(z)$ and the attractive part $w(r) < 0$ of the pair potential:

$$\hat{\gamma}(q) = -\frac{\pi}{2} \iint_{-L_\ell}^{L_v} dz dz' \varrho'(z) \varrho'(z') \int_0^{r_c} dR R^3 \mathcal{J}(qR) w(r) \quad (7)$$

up to terms $O(q^4, C_H q^2)$, where $\mathcal{J}(x) := 4[1 - J_0(x)]/x^2$ with J_0 as a Bessel function of the first kind and $r := \sqrt{R^2 + (z_1 - z_2)^2}$. The limit $q \rightarrow 0$ of eq. (7) corresponds to the Triezenberg–Zwanzig result for γ_0 [3, 45] within the random phase approximation for the direct correlation function, $c(\mathbf{r}_1, \mathbf{r}_2) \approx -w(|\mathbf{r}_1 - \mathbf{r}_2|)/k_B T$. We have evaluated eq. (7) with $\varrho(z)$ from the simulations with $w(r \geq r_0) = V(r) - V(r_c)$ and $w(r < r_0) = V(r_0) - V(r_c)$; $r_0 = 2^{1/6}\sigma$. Over the whole T -range, we find good agreement between the prediction $\hat{\gamma}(q = 0)$ and the data for $\gamma_0(T)$ (fig. 3a). Concerning the q -dependence, however, it turns out (fig. 3b, “DFT”) that $\hat{\gamma}(q; T)/\hat{\gamma}_0(T)$ depends only slightly on T and coincides nearly with the T -independent expression from the sharp-kink approximation, which assumes a step-like variation of $\varrho(z)$ [4]. Equation (7) misses the observed change of the shape of $\gamma(q; T)$ upon varying T and, moreover, yields $\mathcal{K}/\gamma_0 \approx -0.16 < 0$

in stark contrast to $\mathcal{K}(T) > 0$ for all T found above. Note that the neglected term $O(C_H q^2)$, present in DFT [6], could render $\mathcal{K} > 0$.

Recently, Parry *et al.* [26] have revisited the ℓ - v interface within an analytically tractable toy model and compared various definitions of $\gamma(q)$. The approach taken here is motivated by GISAXS experiments and takes the unique interface structure factor $H(q)$ [obtained from $S_{\text{tot}}(q)$] as input for $\gamma(q)$. Theoretical CW descriptions, on the other hand, employ a certain $\mathcal{H}_{\text{int}}[\hat{z}(\mathbf{R}); \hat{\gamma}(q)]$, from which one calculates the fluctuation spectrum $H_{\text{CW}}(q)$ of an idealised sharp surface $\hat{z}(\mathbf{R})$. Within the toy model [26], specifying $\hat{z}(\mathbf{R})$ by a local GDS or any other “crossing criterion” does not generate the expected $H_{\text{CW}}(q)$. Moreover for any choice of $\hat{z}(\mathbf{R})$, the corresponding \mathcal{H}_{int} cannot simply be related to $\gamma(q)$ as given by $H(q)$. The latter summarises the experimentally accessible density fluctuations caused by the presence of the interface, including non-CW (“bulk-like”) terms which cannot be derived from any \mathcal{H}_{int} . [46] This reflects the fact that the representation of a ℓ - v interface by a two-dimensional (2D) manifold renders only an incomplete picture of this inherently 3D object. Within our approach, $\gamma(q)$ provides a good characterisation of the 3D structure of the interface as revealed by scattering experiments.

Conclusions.— We have determined the q -dependent surface tension $\gamma(q; T)$ of a ℓ - v interface covering the full two-phase coexistence region. Our analysis is based on the interface structure factor $H(q)$ and resembles the approach to interpret GISAXS data, thereby avoiding the ambiguous identification of an instantaneous, fluctuating local interface position. The decomposition of fluctuations into bulk and interfacial ones rests on the distinct scaling behaviour of these two contributions upon increasing the penetration depth of scattering waves (in experiments) or the system size (in simulations). As a complication, we found that the (non-singular) leading correction to the bulk scattering intensity contributes to $H(q)$. Our analysis provides a fresh view on GISAXS data for ℓ - v interfaces [7–9] as we do not require any specific model for the bulk scattering; such models can render $\gamma(q)$ meaningless [47]. Instead, the bulk contribution is determined via eq. (5) from the familiar bulk structure factors, to be obtained from independent experiments or simulations. The surface tension $\gamma(q)$ discussed here is fully specified by the two-point density correlation function $G(q, z, z')$ of the inhomogeneous system. However, in general it differs from $\hat{\gamma}(q)$ entering \mathcal{H}_{int} and describing the CW spectrum [26].

Our extensive simulations reveal a pronounced T -dependence of the shape of $\gamma(q; T)$ as a function of q , which upon increasing T , at a certain value q , changes from an almost flat to a convex curve. Our data indicate a positive “bending” coefficient $\mathcal{K} = \gamma_0 \ell^2$ [eq. (6)] for all T , facilitating its interpretation as the square of an emerging length $\ell(T)$. For the simulated LJ fluids, we find a maximum of $\gamma(q; T)$ at wavelengths $2\pi/q_{\text{max}}$ between 3σ and 6σ , which builds up gradually with an up to threefold

enhancement of $\gamma(q_{\max}; T)$ over $\gamma_0(T)$ at $T \approx 0.94 T_c$. At elevated T , measurements of $\gamma(q; T)$ using GISAXS are challenging due to the significant vapour density. However, ℓ - v -like interfaces in suitable colloidal suspensions can be studied well [48] even close to criticality [49], which allows one to analyse $\gamma(q; T)$ along the lines presented here.

ACKNOWLEDGMENTS

We thank R. Evans, K. Mecke, A. Parry, M. Oettel, and P. Tarazona for stimulating discussions and P. Colberg

for many valuable contributions to *HAL's MD package*. Some of the data were produced with the supercomputer *Hydra* of the Max Planck society.

-
- [1] R. Evans, *Adv. Phys.* **28**, 143 (1979).
 [2] J. S. Rowlinson and B. Widom, *Molecular Theory of Capillarity* (Clarendon, Oxford, 1982).
 [3] J. R. Henderson, in *Fundamentals of Inhomogeneous Fluids*, edited by D. Henderson (Marcel Dekker, New York, 1992) Chap. 2, pp. 23–84.
 [4] M. Napiórkowski and S. Dietrich, *Phys. Rev. E* **47**, 1836 (1993).
 [5] A. O. Parry and C. J. Boulter, *J. Phys.: Condens. Matter* **6**, 7199 (1994).
 [6] K. R. Mecke and S. Dietrich, *Phys. Rev. E* **59**, 6766 (1999).
 [7] C. Fradin, A. Braslau, D. Luzet, D. Smilgies, M. Alba, N. Boudet, K. Mecke, and J. Daillant, *Nature* **403**, 871 (2000).
 [8] S. Mora, J. Daillant, K. Mecke, D. Luzet, A. Braslau, M. Alba, and B. Struth, *Phys. Rev. Lett.* **90**, 216101 (2003).
 [9] D. X. Li, B. Yang, B. H. Lin, M. Meron, J. Gebhardt, T. Graber, and S. A. Rice, *Phys. Rev. Lett.* **92**, 136102 (2004).
 [10] T. Bickel, *EPL (Europhys. Lett.)* **106**, 16004 (2014).
 [11] C. Blanc, D. Fedorenko, M. Gross, M. In, M. Abkarian, M. A. Gharbi, J.-B. Fournier, P. Galatola, and M. Nobili, *Phys. Rev. Lett.* **111**, 058302 (2013).
 [12] L. G. MacDowell, J. Benet, N. A. Katcho, and J. M. Palanco, *Adv. Colloid Interface Sci.* **206**, 150 (2014).
 [13] A. Malijeviský and G. Jackson, *J. Phys.: Condens. Matter* **24**, 464121 (2012).
 [14] B. J. Block, S. K. Das, M. Oettel, P. Virnau, and K. Binder, *J. Chem. Phys.* **133**, 154702 (2010).
 [15] S. K. Das and K. Binder, *Phys. Rev. Lett.* **107**, 235702 (2011).
 [16] T. Bieker and S. Dietrich, *Physica A* **252**, 85 (1998).
 [17] E. M. Blokhuis and A. E. van Giessen, *J. Phys.: Condens. Matter* **25**, 225003 (2013).
 [18] M. Müller and L. G. MacDowell, *Macromolecules* **33**, 3902 (2000).
 [19] A. Milchev and K. Binder, *Europhys. Lett.* **59**, 81 (2002).
 [20] R. L. C. Vink, J. Horbach, and K. Binder, *J. Chem. Phys.* **122**, 134905 (2005).
 [21] E. M. Blokhuis, J. Kuipers, and R. L. C. Vink, *Phys. Rev. Lett.* **101**, 086101 (2008).
 [22] E. M. Blokhuis, *J. Chem. Phys.* **130**, 014706 (2009).
 [23] F. Sedlmeier, D. Horinek, and R. R. Netz, *Phys. Rev. Lett.* **103**, 136102 (2009).
 [24] E. Chacón and P. Tarazona, *Phys. Rev. Lett.* **91**, 166103 (2003).
 [25] E. Chacón, E. M. Fernández, and P. Tarazona, *Phys. Rev. E* **89**, 042406 (2014).
 [26] A. O. Parry, C. Rascón, G. Willis, and R. Evans, *J. Phys.: Condens. Matter* **26**, 355008 (2014); A. O. Parry, C. Rascón, and R. Evans, unpublished.
 [27] P. Tarazona, R. Checa, and E. Chacón, *Phys. Rev. Lett.* **99**, 196101 (2007).
 [28] P. Tarazona, E. Chacón, and F. Bresme, *J. Phys.: Condens. Matter* **24**, 284123 (2012).
 [29] S. Dietrich and A. Haase, *Phys. Rep.* **260**, 1 (1995).
 [30] S. Dietrich and H. Wagner, *Z. Phys. B* **56**, 207 (1984).
 [31] F. P. Buff, R. A. Lovett, and F. H. Stillinger, *Phys. Rev. Lett.* **15**, 621 (1965).
 [32] M. S. Wertheim, *J. Chem. Phys.* **65**, 2377 (1976).
 [33] J. D. Weeks, *J. Chem. Phys.* **67**, 3106 (1977).
 [34] F. Höfling and S. Dietrich, unpublished.
 [35] J.-P. Hansen and L. Verlet, *Phys. Rev.* **184**, 151 (1969).
 [36] A. Pelissetto and E. Vicari, *Phys. Rep.* **368**, 549 (2002).
 [37] H. Watanabe, N. Ito, and C.-K. Hu, *J. Chem. Phys.* **136**, 204102 (2012).
 [38] P. H. Colberg and F. Höfling, *Comput. Phys. Commun.* **182**, 1120 (2011); “Highly Accelerated Large-scale Molecular Dynamics package,” Version 0.3, see <http://halmd.org>.
 [39] Employing one Tesla K20Xm GPU (NVIDIA Corp.), a simulation of 447,000 particles at $T^* = 1.15$ over 10^7 steps took about 28 h, including the computation of $I_{\text{tot}}(q; \kappa)$.
 [40] P. de Buyl, P. H. Colberg, and F. Höfling, *Comput. Phys. Commun.* **185**, 1546 (2014).
 [41] We emphasise that $S_b(q) \neq \rho_\ell L_\ell S_\ell(q) + \rho_v L_v S_v(q)$.
 [42] Note that the vapour contribution has been neglected in refs. [21–23], which at small q amounts to modifying $\gamma(q)$ by a term $O(q^2)$.
 [43] A. O. Parry and R. Evans, *Phys. Rev. A* **46**, 5282 (1992).
 [44] M. Hasenbusch and K. Pinn, *Phys. A* **192**, 342 (1993).
 [45] D. G. Triezenberg and R. Zwanzig, *Phys. Rev. Lett.* **28**, 1183 (1972).
 [46] The non-CW terms in $H(q)$ must not be confused with $S_b(q)$, the latter describing bulk fluctuations in the absence of an interface.

- [47] M. Paulus, C. Gutt, and M. Tolan, *Phys. Rev. B* **78**, 235419 (2008).
- [48] D. G. A. L. Aarts, M. Schmidt, and H. N. W. Lekkerkerker, *Science* **304**, 847 (2004).
- [49] C. P. Royall, D. G. A. L. Aarts, and H. Tanaka, *Nature Phys.* **3**, 636 (2007).